

ASME Journal of Applied Mechanics Online journal at:

https://asmedigitalcollection.asme.org/appliedmechanics



Mechanics of Tunable Adhesion With Surface Wrinkles

Teng Zhang

Department of Mechanical and Aerospace Engineering; BioInspired Syracuse, Syracuse University, Syracuse, NY 13244 e-mail: tzhang48@syr.edu

Surface wrinkles have emerged as a promising avenue for the development of smart adhesives with dynamically tunable adhesion, finding applications in diverse fields, such as soft robots and medical devices. Despite intensive studies and great achievements, it is still challenging to model and simulate the tunable adhesion with surface wrinkles due to roughened surface topologies and pre-stress inside the materials. The lack of a mechanistic understanding hinders the rational design of these smart adhesives. Here, we integrate a lattice model for nonlinear deformations of solids and nonlocal interaction potentials for adhesion in the framework of molecular dynamics to explore the roles of surface wrinkles on adhesion behaviors. We validate the proposed model by comparing wrinkles in a neo-Hookean bilayer with benchmarked results and reproducing the analytical solution for cylindrical adhesion. We then systematically study the pull-off force of the wrinkled surface with varied compressive strains and adhesion energies. Our results reveal the competing effect between the adhesion-induced contact and the roughness due to wrinkles on enhancing or weakening the adhesion. Such understanding provides guidance for tailoring material and geometry as well as loading wrinkled surfaces for different applications. [DOI: 10.1115/1.4062699]

Keywords: tunable adhesion, ruga, wrinkles, lattice models, elasticity, structures

1 Introduction

Smart adhesives with tunable adhesion [1–5] play important roles in various applications as diverse as robotics [6–8], small-object manipulations [9–11], and medical devices [12–14]. Surface wrinkles have been shown very promising to dynamically tune adhesion [15–24] via the control of surface morphologies, such as wrinkle wavelength and amplitude. These smart adhesives based on wrinkles are highly appealing due to their straightforward fabrication process, compatibility with a wide range of materials, ease of manipulation, and ability to be used repeatedly. For example, Chan et al. reported controllable adhesion enabled by swelling-induced surface wrinkles in elastomer and found that wrinkles can enhance the adhesion when the wrinkle wavelength is smaller than a critical value [15]. Lin et al. tuned the adhesion of a wrinkled bilayer elastomeric structure via mechanical stretching and applied it to repeatedly pick and release a glass ball [16].

To rationally design surface wrinkles for smart adhesives, substantial effort has been devoted to the mechanics modeling and simulations of the process [16,20]. Most existing studies are based on simplified models because the highly nonlinear interactions between the indenter and the wrinkled substrate pose great challenges to mechanistic understanding. The scientific challenges stem from several coupled factors introduced by surface wrinkles that will synergically affect the adhesion property. First, wrinkles

modify the surface roughness, which alone has been shown to play a very important role in determining adhesion. Second, non-uniform initial stresses, before interacting with an indenter, are the driving force of the wrinkle formation and required to be included in the adhesion analysis. Third, material heterogeneities are necessary to form wrinkles and add more complicity to the problem. Fourth, the top layer of the surface wrinkles generally undergoes large bending deformation, making analytical solutions difficult to obtain. Although the surface roughness effect on adhesion has been extensively studied [25–38] and indeed offered important insights into the wrinkled adhesion, more effort is still needed to uncover the coupling roles of these factors in tuning adhesion with controlled wrinkles.

Numerical simulations are almost inevitable to address the above challenges. This further brings another technique challenge due to three separated length scales involved in the simulations, including contact radius, wrinkle wavelength, and the lattice space. To correctly capture this multiscale character, large-scale simulations are necessary and pose challenges for numerical analysis. To address the scientific and technique challenges, we develop a modeling framework by coupling a lattice model [39–43] for the nonlinear deformation of the substrate and film and Lennard–Jones (L–J) pair interactions for interfacial adhesion. The lattice model has been shown to be able to accurately capture the nonlinear nearly incompressible deformation of neo-Hookean solids [41-43]. L-J potentials have been widely used to describe interfacial adhesion [32,38,44–46]. We integrate them in large-scale atomic/molecular massively parallel simulator (LAMMPS) [47], a powerful parallel simulation platform, to explicitly model the multiscale and nonlocal interactions.

The rest of the paper is organized as follows. Section 2 introduces the simulation model, including the lattice model and the L-J

Manuscript received May 28, 2023; final manuscript received June 1, 2023; published online August 7, 2023. Assoc. Editor: Ruike Renee Zhao.

This paper is dedicated to Professor Kyung-Suk Kim, for his contributions to experimental and theoretical micro and nano-mechanics, and in celebration of his 70th birthday.

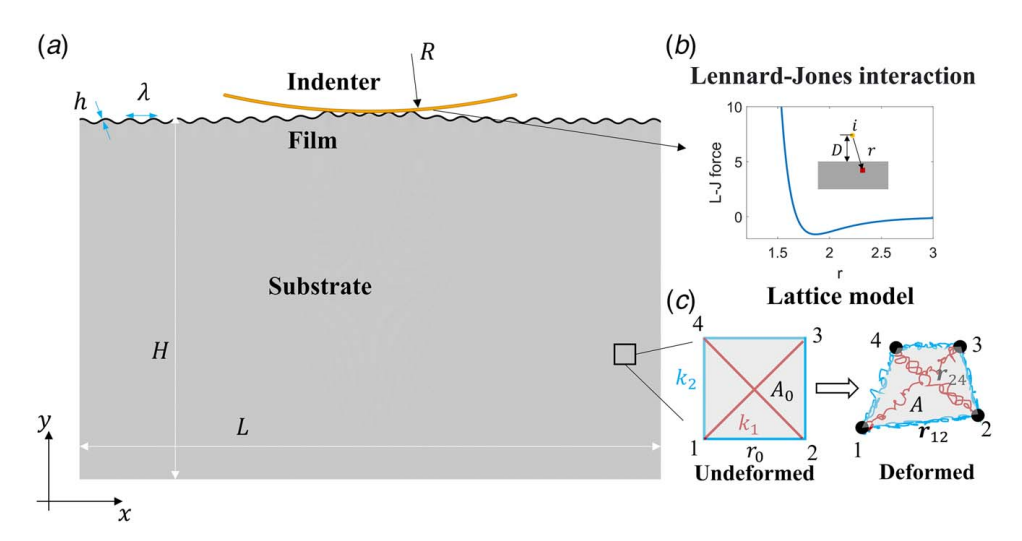


Fig. 1 The schematic of the simulation framework: (a) a wrinkled bilayer interacting with an indenter, where the substrate has a length of L and depth of H, the film has a length of L and thickness of h, the wrinkle wavelength is λ , and the indenter radius is R and (b) The Lennard–Jones interaction for adhesion. (c) The lattice model for the elastic bodies.

potentials. Model validation with benchmarked wrinkle formation and evolution is presented in Sec. 3. Section 4 is dedicated to comparing the two-dimensional (2D) cylindrical adhesion from simulations and analytical solutions. Section 5 presents examples of adhesion with surface wrinkles and studies the pull-off force of the wrinkled surface with varied compressive strains and adhesion energies. Finally, some concluding remarks are given in Sec. 6.

2 Simulation Model

In this paper, we focus on 2D structures under the plane strain condition (Fig. 1(a)). We use the lattice model to describe the nonlinear deformation of the substrate and film and describe the adhesion between an indenter and elastic bodies with Lennard–Jones potential, which is both available in LAMMPS.

To model the adhesion, we employ the standard 12/6 Lennard–Jones (L–J) potential, defining a pair interaction between particles on the indenter and in the elastic body (Fig. 1(b)). The potential energy between two particles is given by

$$V_{LJ} = 4\varepsilon \left[\left(\frac{\sigma}{r} \right)^{12} - \left(\frac{\sigma}{r} \right)^{6} \right], \quad r < r_{c}$$
 (1)

where r is the distance between the two particles, ε is the depth of the energy well, σ is the zero potential energy distance, and r_c is the cutoff distance of the interaction. Here, we only model the indenter of a single layer of particles, which are uniformly distributed on a cylindrical surface. To map the pair interaction into the effective adhesion energy, one can first compute the energy density of the integral of a solid line and a solid half-space [45], which is a function of the distance between the line and the surface, D (Fig. 1(b)). The absolute value of the minimum energy density will give the effective adhesion energy. Here, we extract the effective adhesion energy by comparing the simulation results with the classical solutions of cylindrical adhesion to take the discrete effects into account.

Since the substrate and film are regular rectangles, we adopt a square lattice with the edge length $r_0 = 1$ to simplify the model. The strain energy inside the square element can be computed via the energies of the six springs and the area change (Fig. 1(c)) as [41]

$$U_E = \frac{1}{2}k_1(r_{13}^2 + r_{24}^2) + \frac{1}{2}k_2(r_{12}^2 + r_{23}^2 + r_{34}^2 + r_{14}^2) + \frac{1}{2}\left(K - \frac{2G}{3}\right)\left(\ln\left(\frac{A}{A_0}\right)\right)^2 - G\ln\left(\frac{A}{A_0}\right)$$
(2)

where G is the shear modulus, K is the bulk modulus, $k_1 = \frac{1}{3}G$, and $k_2 = \frac{1}{6}G$ are the spring stiffnesses. It is important to note that edge lattices (e.g., r_{12} , r_{14} in Fig. 1(c)) within the bulk of the materials are shared by two elements, resulting in a combined contribution to the spring stiffness, effectively yielding a stiffness value of $2k_2$. The same framework can also be applied to irregular lattice shapes [41], although it is not necessary in the current work.

We adopt the "metal" unit system in LAMMPS. To keep the description simple, we will omit units of different variables in the following discussion. Since we only focus on the static loading cases, time scales do not play important roles in our studies. To compare the simulated results with real-world structures, we can normalize the stress scale with the substrate shear modulus (G), the length scale with the lattice edge (r_0) , the force scale with Gr_0^2 , and the energy scale as Gr_0^3 .

3 Model Validation With Wrinkle Simulations

The lattice model has been applied to simulate the nonlinear deformation of neo-Hookean solids [41-43]. To further test its applicability to the adhesion of wrinkled surfaces, we first apply the lattice model to simulate surface wrinkle formation and evolution of a bilayer structure (Fig. 2) and validate our model with benchmark solutions. The substrate has a length of L_0 and height of H_0 at the undeformed configuration, and the film has a thickness h of 2. The shear moduli of the substrate (G_s) and film (G_f) are 2 and 200, respectively. The Lame constant $\left(K - \frac{2G}{3}\right)$ is set to be 20 times the shear modulus to model the nearly incompressible condition of the solid material. The periodical boundary condition is applied to the left and right surface along the x direction. Here, we choose L_0 as 337 to have eight wrinkles in the simulation box. The substrate is thick enough (300) to approximate the semi-infinite condition. The compressive loading is applied by gradually deforming the simulation box along the x direction. Since we adopt the explicit time integration in LAMMPS, we pause the deform loading at each 0.01 incremental strain and further run a long period of relaxation simulation after each strain increment to ensure that the structure is in equilibrium. The details of the simulation can be found in the LAMMPS job script, which can be found in the link in the Data Availability Statement.

We present a few simulation snapshots in Fig. 2, which give the critical wrinkling strain as 0.24 and the onset wrinkle wavelength as 41.11. According to the classical wrinkle instability of a bilayer structure, the critical wrinkle strain and wavelength are [48]

$$\varepsilon_w = \frac{1}{4} \left(\frac{3G_s}{G_f} \right)^{2/3} \text{ and } \lambda_w = 2\pi h \left(\frac{G_f}{3G_s} \right)^{1/3}$$
 (3)

For the current material and geometrical properties $(\frac{G_i}{G_i} = 100)$ and h = 2), we can obtain the theoretical critical strain and wavelength as 0.241 and 40.4, respectively, which are in great agreement with our simulated critical strain (0.24) and wavelength (41.11). We also successfully predict periodical doubling when the compressive strain reaches 0.2 [48–51]. The detailed wrinkle evolution can be found in Supplementary Video 1 (available in the Supplemental Materials on the ASME Digital Collection).

4 Model Validation With Two-Dimensional Cylindrical Adhesion

We next compare our simulations of 2D adhesion of cylindrical indenter with the analytical solution [52,53], derived from the same framework of the Johnson–Kendall–Roberts (JKR) model [54]. In the schematics of the modeling setup (Fig. 3(a)), we omit the global substrate and only focus on the local structures of the

indenter and substrate near the contact parts. The indenter is a circular arc with a radius of R, varying from 90 to 400. Symmetry boundary condition is applied to the left and right surface along the x direction. Here, we set the substrate length as $L_0 = 1000$, which is much larger than the contact radius (<100), to eliminate the boundary effect. The substrate material has a shear modulus of 2 and a Lame constant of 40. The indenter is only a single layer of particles with an equal spacing of 1. The parameters of the L–J potential are $\varepsilon = 0.5$, $\sigma = 1.5$, and $r_c = 6$ (Fig. 3(a)). We set a large cutoff value to capture the nonlocal adhesive interaction.

The simulation contains two steps, including indentation and retraction. In the indentation step, we also employ the moving and relaxing strategy to the indenter to search for an equilibrium solution along the loading path. Initially, the indenter is positioned 6 above the substrate to ensure a minimal interaction between the indenter and the substrate. The indenter is then moved toward the substrate with an increment displacement of 0.05. We hold the indenter and let the system run to minimize the total energy. After equilibrium is reached, we repeat the previous process. In the retraction step, we reverse the displacement direction of the indenter and keep the other settings the same.

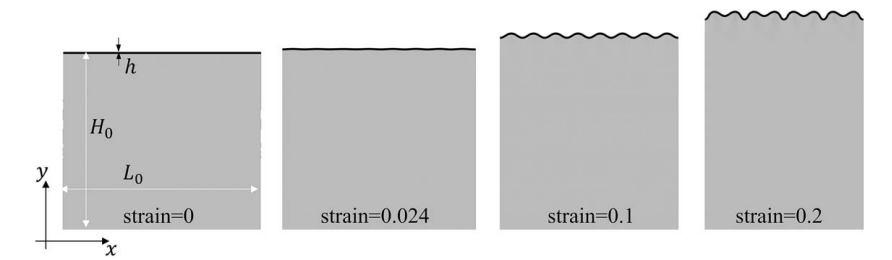


Fig. 2 Simulated wrinkle formation and evolution using the lattice model

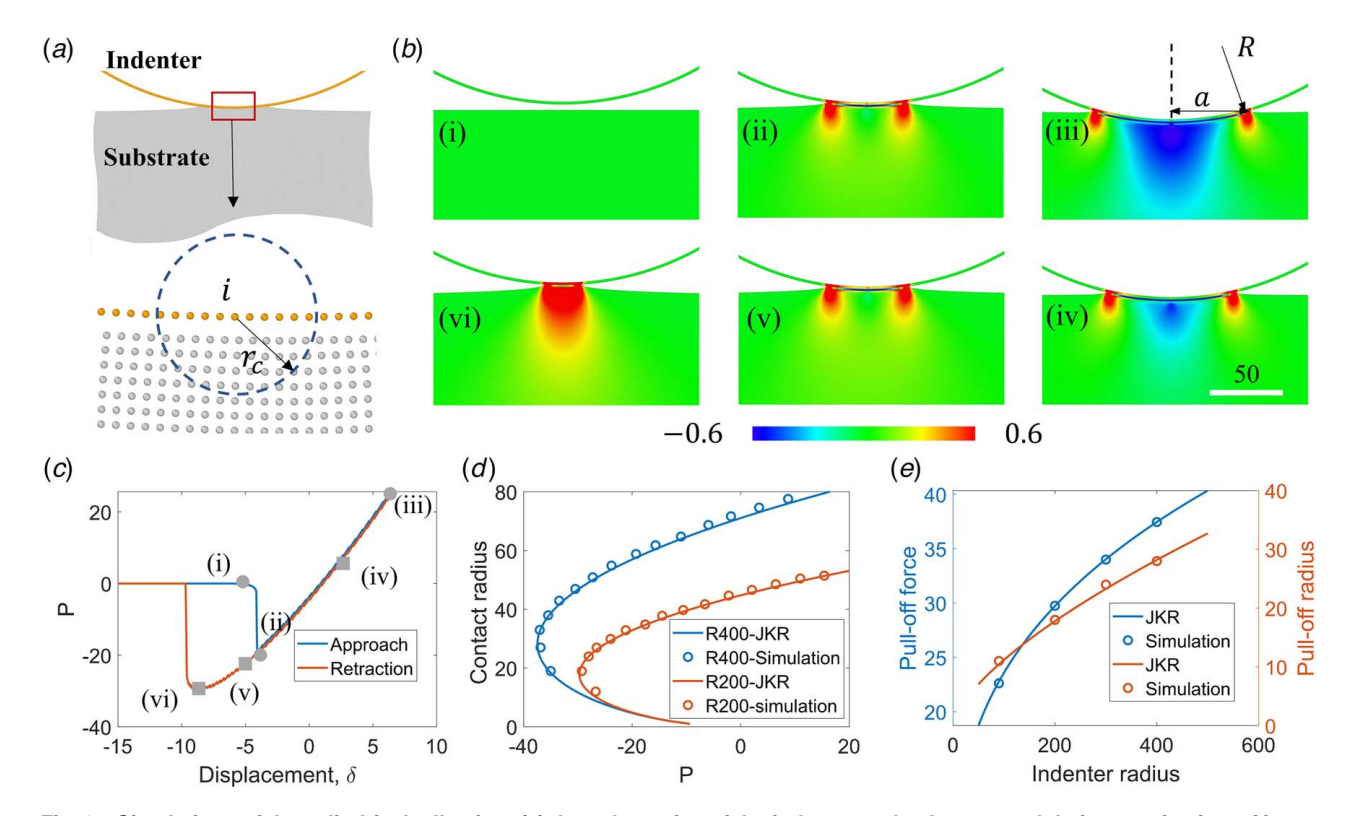


Fig. 3 Simulations of the cylindrical adhesion: (a) the schematics of the indenter and substrate and their zoom-in view of interactions, (b) snapshots of the deformation and stress during the approach and retraction steps, (c) contact force and indentation depth relationship, (d) contact radius in terms of the contact force with different indenter radii, and (e) pull-off force and radius in terms of the indenter radii. Color in (b) indicates σ_{vv} .

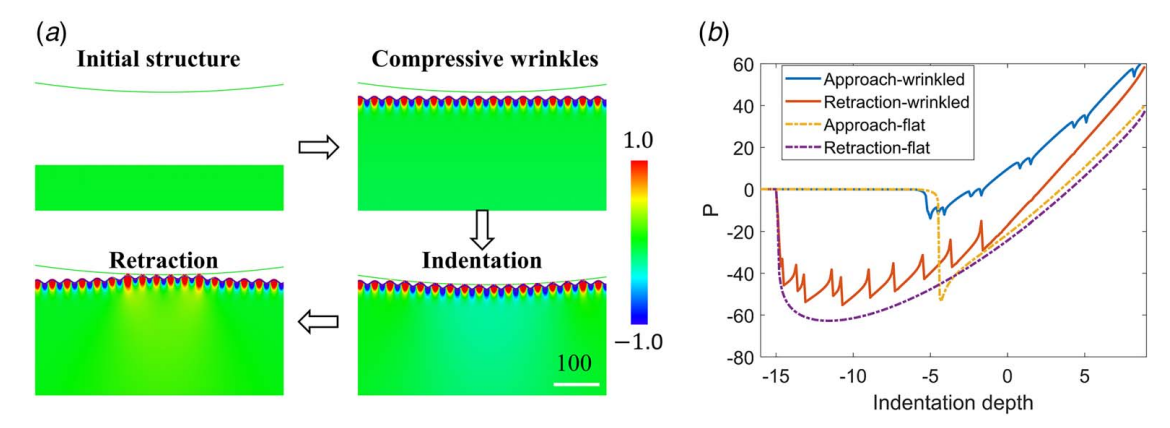


Fig. 4 Adhesion simulation of the wrinkled surface: (a) simulation steps and (b) contact force in terms of the indentation depth for wrinkled and flat cases. Color in (a) indicates σ_{vv} .

For a representative case with R = 200, both pull-in and pull-off instabilities are successfully captured by our model, ss shown in Figs. 3(b) and 3(c), which can also be seen from the Supplementary Video 2 (available in the Supplemental Materials). In addition, stress contractions are clearly seen at the interfacial tips. Here, we report viral stresses, which are easy to compute in the molecular dynamics framework and related to Cauchy stress at the continuum level [55,56]. We further seek quantitative comparison with the analytical solutions of the cylindrical adhesion, which predicts the relationship between the contact force (P) and radius (a) as [53]

$$P = (\pi G a^2)/R - 2\sqrt{2\pi G a \gamma} \tag{4}$$

where G is the shear modulus, R is the indenter radius, and γ is the adhesion energy. In this analytical formula, we assume the material is fully incompressible (e.g., Poisson's ratio as 0.5). We fit the simulation results of the P-a relationship in Eq. (4) to extract the adhesion energy (Fig. 3(d)). This specific case gives us $\gamma = 1.76$. To verify the value is an interfacial property for given simulation parameters, we vary the indenter radii in simulation and show the same adhesion energy (1.76) can accurately predict their adhesion behaviors. We focus on the comparison of the pull-off force and the corresponding contact radius. Through minimizing Eq. (4), the theoretical pull-off force and radius can be expressed as [53]

$$P_{cr} = -3\left(\frac{\pi G \gamma^2 R}{4}\right)^{\frac{1}{3}} \tag{5}$$

$$a_{cr} = \left(\frac{\gamma}{2\pi G}\right)^{1/3} R^{2/3} \tag{6}$$

Here, we take the absolute value of the minima of the contact force. Both simulated and analytical results are presented in Fig. 3(e), showing great agreement with each other.

5 Tunable Adhesions With Wrinkled Surfaces

After we validate the lattice model simulations with benchmark solutions of surface wrinkles and 2D JKR solution, we are ready to simulate the adhesion of wrinkled surfaces. We first run a representative case to demonstrate the features of the adhesion at the wrinkled surface. Then, we systematically vary key parameters, including the compressive strain and the adhesion energy, to quantify their effects on the tunable adhesion.

5.1 Demonstration of Adhesion of Wrinkled Surfaces. We demonstrate the adhesion of the wrinkled surface of a bilayer structure with the same material properties (e.g., $(\frac{G_f}{G_s} = 100 \text{ and } G_s = 2)$ and film thickness (h = 2) as the wrinkle simulation in Sec. 3. To

capture the multiscale nature of the problem, we set the indenter radius as 2000, much larger than the wavelength (\sim 40). Accordingly, we increase the substrate length and depth to 2022 and 1000, respectively, to approximate the semi-infinite space. Periodical boundary condition is applied to the x direction. The bottom of the surface is constrained along the y direction. The maximum contact radius is around 400, much smaller than the substrate length, although the indenter radius is comparable to the length. The parameters of the L–J potential are $\varepsilon = 0.5$, $\sigma = 1.5$, and $r_c = 6$.

The simulation consists of three steps, including compressive wrinkling, indentation, and retraction (Fig. 4(a)). In this example, we apply 15% compressive strain to trigger wrinkles. A dynamic process can be seen in Supplementary Video 3 (available in the Supplemental Materials), from which we can observe discontinuous detachments of individual wrinkles from the indenter. Correspondingly, the contact force will have a jump due to the sudden release of a contact point (Fig. 4(b)). On the contrary, the contact force changes smoothly for the flat surface. Similar force jumps have been experimentally observed and theoretically predicted in rough adhesion [29,31,33,36,38]. Another interesting observation is that pull-in instability is largely suppressed at the wrinkled surface. This can be attributed to the contact splitting that prevents the continuous growth of the contact area when the indenter approaches the substrate.

5.2 Adhesion of Surfaces With Varied Wrinkle Amplitude and Morphology. To gain a comprehensive understanding of the impact of surface wrinkles on adhesion, we conduct simulations of various bilayer structures under different compressive strains. This will lead to variations of wrinkle amplitude and wavelength (Fig. 5(a)) and morphology, such as sinusoidal wrinkles at small strains and periodical doubling at large strains (Fig. 2). In addition, stress states in the structure will also be changed, making it more complicated than a purely geometrical variation. We also increase the film thickness from 2 to 4, which gives a higher resolution of the wrinkle simulation. It should be noted that the bending stiffness of the film also increases, except for the changes in the wrinkle wavelength. The parameters of the L–J potential are $\varepsilon = 0.1$, $\sigma = 1.5$, and $r_c = 6$.

We present plots of contact forces in terms of indentation depths for three strain values (0%, 5%, and 10%) in Fig. 5(b). Discrete force jumps can be observed for wrinkled surfaces, consistent with the simulations in Sec. 5.1. Compared to the flat bilayer structure, the wrinkle bilayer has a larger pull-off force at 5% compressive strain and a smaller pull-off force at 10% compressive strain (Fig. 5(b)). At 5% strain, the wrinkle amplitude is small so that the real contact area is enlarged, leading to an enhanced adhesion (left in Fig. 5(c)), which has been reported for rough surfaces and wrinkled surfaces [15,21,31,38]. At 10% strain, the wrinkle

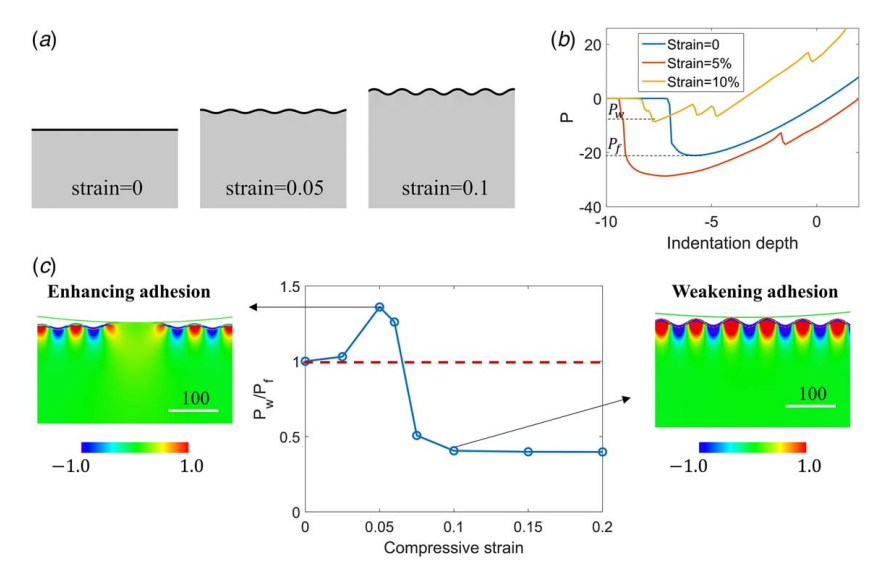


Fig. 5 Adhesion of surfaces with varied wrinkle amplitude: (a) representative configuration of the bilayer structure at different compressive strains, (b) contact force in terms of the indentation depth at different compressive strains, and (c) normalized pull-off force in terms of the compressive strain and the configurations of enhanced and weakened adhesion. Color in (c) indicates σ_{yy} .

amplitude is large and thus reduces the real contact to a few contact points, which weakens the adhesion (right in Fig. 5(c)). Similar weakening adhesion has been shown in several wrinkled surfaces [16,24]. We further continuously vary the compressive strain from 0% to 20% and show surface wrinkles first enhance and then decrease the adhesion, which reaches a plateau when the strain value is larger than 10% (middle in Fig. 5(c)). It is also interesting to note that periodical doubling (20% compressive strain) will not change the adhesion a lot compared to the sinusoidal wrinkles.

5.3 Adhesion of Surfaces With Varied Adhesion Strength.

The previous simulations are based on a fixed adhesion energy and varied wrinkle amplitudes and morphologies. It is also important to examine the adhesion behaviors of a given wrinkled structure at different adhesion energy. Here, we fix the compressive strain value as 10% and gradually change the depth of the energy well, ε , in the L–J potential to tune the adhesion energy. Representative adhesive interactions with different ε are shown in Fig. 6(a). As shown in Figs. 6(b) and 6(c), surface wrinkles reduce the pull-off force for small ε and increase the pull-off

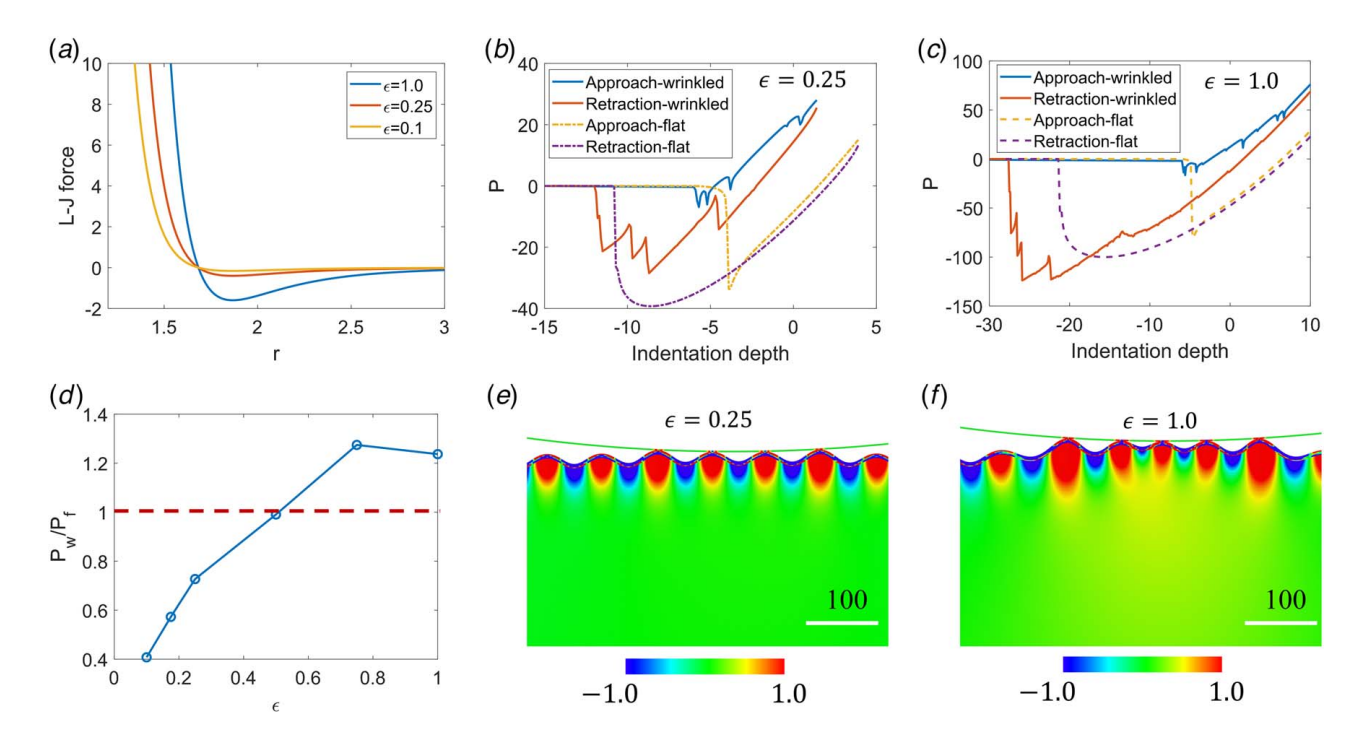


Fig. 6 Adhesion of a wrinkled surface with adhesion energy: (a) Representative interaction forces of different depths of the energy well, ε , in the L–J potential. (b) Contact force in terms of the indentation depth for $\varepsilon = 0.25$. (c) Contact force in terms of the indentation depth for $\varepsilon = 1.0$. (d) Normalized pull-off force in terms of ε . (e) Simulation snapshot at the pull-off instability point for $\varepsilon = 0.25$. (f) Simulation snapshot at the pull-off instability point for $\varepsilon = 1.0$. Color in (e) and (f) indicates σ_{vy} .

force for large ε . For the given wrinkled surface, we identify a critical $\varepsilon \approx 0.5$ for enhancing or weakening the adhesion. The weakening mechanism is the reduction of the contact area and consistent for small ε (0.1 for Figs. 5(ε) and 0.25 for Fig. 6(ε)). For large ε and wrinkles with large amplitudes, increased adhesion can also be achieved even without the increase in the contact area (Fig. 6(ε)). This provides another adhesion-enhancing mechanism and is likely due to the crack trapping effect, which has been observed in the adhesion of substrate with fibrillar structures [57] and wavy surfaces [31].

6 Conclusions

We have developed a simple yet versatile simulation method that enables us to comprehensively understand the mechanisms underlying the enhancement and weakening of adhesion in wrinkled surfaces. Our model is based on the integration of a lattice model for deformable wrinkled surface and substrate and L-J nonlocal interactions for adhesion in the framework of molecular dynamics. All the simulations are performed with LAMMPS, which is highly efficient in parallel simulations and thus powerful to explore complicated adhesion problems. We first validated the proposed model through benchmark simulations of wrinkles in a neo-Hookean bilayer and cylindrical adhesion. We then systematically study the pull-off force of the wrinkled surface with varied compressive strains and effective adhesion energies for flat substrate. Our simulations can successfully capture the pull-in and pull-off instabilities of the adhesion at flat surfaces and force jumps of the adhesion at wrinkled surfaces. Our results further reveal the competing effect between the adhesion-induced contact and the roughness due to wrinkles on enhancing or weakening the adhesion. The weakened adhesion happens for cases with large-amplitude wrinkles and low adhesion energies, due to the decrease of the contact area. Two possible adhesion-enhancing mechanisms are identified when wrinkle amplitudes are small and adhesion energies are high, including the increase in the contact area and crack trapping. Our findings are in good agreement with previous studies of the adhesion of wrinkled surfaces and rough surfaces.

The developed modeling framework also opens opportunities to investigate the tunable adhesion of other surfaces with different instability patterns. For example, hierarchical wrinkles [58–60] have been successfully fabricated and shown to provide more freedom to tune the wetting properties and structure light. The multilevel wrinkles may have synergistic effects on enhancing or weakening the adhesion, where our simulations can be very helpful to identify the critical design parameters. 2D Surface wrinkles [61-67] exhibit even richer controlled surface morphologies and thus provide more freedom to tune the adhesion. 3D Lattice models have been implemented in LAMMPS [68] and are ready to study the adhesion of 2D wrinkled surfaces. Surface wrinkles are only a subset of ruga phases [51,69,70], which also include creases [71-73], folds [74,75], or ridges [48,76]. It will be of great interest in exploring the tunability of adhesion of different ruga phases.

Acknowledgment

We thank Dr. Guangchao Wan for the valuable discussion. The research was supported by the National Science Foundation (NSF) under Grant No. NSF CMMI-1847149. Simulations were performed at the Expanse cluster (Award No. TG-MSS170004) in the Advanced Cyberinfrastructure Coordination Ecosystem: Services & Support (ACCESS).

Conflict of Interest

There are no conflicts of interest.

Data Availability Statement

The data and information that support the findings of this article are freely available. ¹

References

- Arzt, E., Quan, H., McMeeking, R. M., and Hensel, R., 2021, "Functional Surface Microstructures Inspired by Nature–From Adhesion and Wetting Principles to Sustainable New Devices," Prog. Mater. Sci., 120, p. 100823.
- [2] Croll, A. B., Hosseini, N., and Bartlett, M. D., 2019, "Switchable Adhesives for Multifunctional Interfaces," Adv. Mater. Technol., 4(8), p. 1900193.
- [3] Linghu, C., Liu, Y., Tan, Y. Y., Sing, J. H. M., Tang, Y., Zhou, A., Wang, X., Li, D., Gao, H., and Hsia, K. J., 2023, "Overcoming the Adhesion Paradox and Switchability Conflict on Rough Surfaces With Shape-Memory Polymers," Proc. Natl. Acad. Sci. U. S. A., 120(13), p. e2221049120.
- [4] Tatari, M., Mohammadi Nasab, A., Turner, K. T., and Shan, W., 2018, "Dynamically Tunable Dry Adhesion via Subsurface Stiffness Modulation," Adv. Mater. Interfaces, 5(18), p. 1800321.
- [5] Cho, H., Wu, G., Christopher Jolly, J., Fortoul, N., He, Z., Gao, Y., Jagota, A., and Yang, S., 2019, "Intrinsically Reversible Superglues via Shape Adaptation Inspired by Snail Epiphragm," Proc. Natl. Acad. Sci., 116(28), pp. 13774–13779.
- [6] Kim, S., Spenko, M., Trujillo, S., Heyneman, B., Santos, D., and Cutkosky, M. R., 2008, "Smooth Vertical Surface Climbing With Directional Adhesion," IEEE Trans. Rob., 24(1), pp. 65–74.
- [7] Tang, Y., Zhang, Q., Lin, G., and Yin, J., 2018, "Switchable Adhesion Actuator for Amphibious Climbing Soft Robot," Soft Rob., 5(5), pp. 592–600.
- [8] Duan, W., Yu, Z., Cui, W., Zhang, Z., Zhang, W., and Tian, Y., 2023, "Bio-Inspired Switchable Soft Adhesion for the Boost of Adhesive Surfaces and Robotics Applications: A Brief Review," Adv. Colloid Interface Sci., 313, p. 102862.
- [9] Meitl, M. A., Zhu, Z.-T., Kumar, V., Lee, K. J., Feng, X., Huang, Y. Y., Adesida, I., Nuzzo, R. G., and Rogers, J. A., 2006, "Transfer Printing by Kinetic Control of Adhesion to an Elastomeric Stamp," Nat. Mater., 5(1), pp. 33–38.
- [10] Zhang, X., Wang, Y., Tian, Z., Samri, M., Moh, K., McMeeking, R. M., Hensel, R., and Arzt, E., 2022, "A Bioinspired Snap-Through Metastructure for Manipulating Micro-Objects," Sci. Adv., 8(46), p. eadd4768.
- [11] Wan, G., Tang, Y., Turner, K. T., Zhang, T., and Shan, W., 2023, "Tunable Dry Adhesion of Soft Hollow Pillars Through Sidewall Buckling Under Low Pressure," Adv. Funct. Mater., 33(2), p. 2209905.
- [12] Bae, W.-G., Kim, D., and Suh, K.-Y., 2013, "Instantly Switchable Adhesion of Bridged Fibrillar Adhesive via Gecko-Inspired Detachment Mechanism and Its Application to a Transportation System," Nanoscale, 5(23), pp. 11876–11884.
- [13] Chen, X., Yuk, H., Wu, J., Nabzdyk, C. S., and Zhao, X., 2020, "Instant Tough Bioadhesive With Triggerable Benign Detachment," Proc. Natl. Acad. Sci., 117(27), pp. 15497–15503.
- [14] Jinkins, K. R., Li, S., Arafa, H., Jeong, H., Lee, Y. J., Wu, C., Campisi, E., et al., 2022, "Thermally Switchable, Crystallizable Oil and Silicone Composite Adhesives for Skin-Interfaced Wearable Devices," Sci. Adv., 8(23), pp. eabo0537.
- [15] Chan, E. P., Smith, E. J., Hayward, R. C., and Crosby, A. J., 2008, "Surface Wrinkles for Smart Adhesion," Adv. Mater., 20(4), pp. 711–716.
- [16] Lin, P.-C., Vajpayee, S., Jagota, A., Hui, C.-Y., and Yang, S., 2008, "Mechanically Tunable Dry Adhesive From Wrinkled Elastomers," Soft Matter, 4(9), pp. 1830–1835.
- [17] Jeong, H. E., Kwak, M. K., and Suh, K. Y., 2010, "Stretchable, Adhesion-Tunable Dry Adhesive by Surface Wrinkling," Langmuir, 26(4), pp. 2223–2226.
- [18] Chan, E. P., Karp, J. M., and Langer, R. S., 2011, "A "Self-Pinning" Adhesive Based on Responsive Surface Wrinkles," J. Polym. Sci., Part B: Polym. Phys., 49(1), pp. 40–44.
- [19] Kundu, S., Davis, C. S., Long, T., Sharma, R., and Crosby, A. J., 2011, "Adhesion of Nonplanar Wrinkled Surfaces," J. Polym. Sci., Part B: Polym. Phys., 49(3), pp. 179–185.
- [20] Davis, C. S., and Crosby, A. J., 2011, "Mechanics of Wrinkled Surface Adhesion," Soft Matter, 7(11), pp. 5373–5381.
- [21] Davis, C. S., Martina, D., Creton, C., Lindner, A., and Crosby, A. J., 2012, "Enhanced Adhesion of Elastic Materials to Small-Scale Wrinkles," Langmuir, 28(42), pp. 14899–14908.
- [22] Rahmawan, Y., Chen, C.-M., and Yang, S., 2014, "Recent Advances in Wrinkle-Based Dry Adhesion," Soft Matter, 10(28), pp. 5028–5039.
- [23] Zhang, T., Zhang, Z., Kim, K.-S., and Gao, H., 2014, "An Accordion Model Integrating Self-Cleaning, Strong Attachment and Easy Detachment Functionalities of Gecko Adhesion," J. Adhes. Sci. Technol., 28(3–4), pp. 226– 239
- [24] Wang, Y., and Xiao, J., 2017, "Programmable, Reversible and Repeatable Wrinkling of Shape Memory Polymer Thin Films on Elastomeric Substrates for Smart Adhesion," Soft Matter, 13(31), pp. 5317–5323.
- [25] Fuller, K., and Tabor, D., 1975, "The Effect of Surface Roughness on the Adhesion of Elastic Solids," Proc. R. Soc. A, 345(1642), pp. 327–342.
- [26] Maugis, D., 1996, "On the Contact and Adhesion of Rough Surfaces," J. Adhes. Sci. Technol., 10(2), pp. 161–175.

¹https://github.com/tengzhang48/Mechanics_Wrinkle_Adhesion_Lattice_Simulations

- [27] Hui, C., Lin, Y., Baney, J., and Kramer, E., 2001, "The Mechanics of Contact and Adhesion of Periodically Rough Surfaces," J. Polym. Sci., Part B: Polym. Phys., 39(11), pp. 1195-1214.
- [28] Persson, B., 2002, "Adhesion Between an Elastic Body and a Randomly Rough Hard Surface," Eur. Phys. J. E, 8(4), pp. 385-401.
- [29] Guduru, P., 2007, "Detachment of a Rigid Solid From an Elastic Wavy Surface: Theory," J. Mech. Phys. Solids., 55(3), pp. 445-472.
- [30] Pastewka, L., and Robbins, M. O., 2014, "Contact Between Rough Surfaces and a Criterion for Macroscopic Adhesion," Proc. Natl. Acad. Sci., 111(9), pp. 3298-
- [31] Guduru, P., and Bull, C., 2007, "Detachment of a Rigid Solid From an Elastic Wavy Surface: Experiments," J. Mech. Phys. Solids., 55(3), pp. 473–488.
- [32] Jin, C., Khare, K., Vajpayee, S., Yang, S., Jagota, A., and Hui, C.-Y., 2011, "Adhesive Contact Between a Rippled Elastic Surface and a Rigid Spherical Indenter: From Partial to Full Contact," Soft Matter, 7(22), pp. 10728–10736.
- [33] Kesari, H., and Lew, A. J., 2011, "Effective Macroscopic Adhesive Contact Behavior Induced by Small Surface Roughness," J. Mech. Phys. Solids., 59(12), pp. 2488-2510.
- [34] Jin, F., Guo, X., and Wan, Q., 2016, "Revisiting the Maugis-Dugdale Adhesion Model of Elastic Periodic Wavy Surfaces," ASME J. Appl. Mech., 83(10), p. 101007
- [35] Li, Q., and Kim, K. S., 2009, "Micromechanics of Rough Surface Adhesion: A
- Homogenized Projection Method," Acta Mech. Solida Sin., 22(5), pp. 377–390. [36] Deng, W., and Kesari, H., 2019, "Depth-Dependent Hysteresis in Adhesive Elastic Contacts at Large Surface Roughness," Sci. Rep., 9(1), p. 1639.
- [37] Papangelo, A., and Ciavarella, M., 2020, "A Numerical Study on Roughness-Induced Adhesion Enhancement in a Sphere With an Axisymmetric Sinusoidal Waviness Using Lennard-Jones Interaction Law," Lubricants, 8(9), p. 90.
- [38] Zhu, Y., Zheng, Z., Zhang, Y., Wu, H., and Yu, J., 2021, "Adhesion of Elastic Wavy Surfaces: Interface Strengthening/Weakening and Mode Transition Mechanisms," J. Mech. Phys. Solids., 151, p. 104402.
- [39] Buxton, G. A., and Balazs, A. C., 2002, "Lattice Spring Model of Filled Polymers and Nanocomposites," J. Chem. Phys., 117(16), pp. 7649–7658. [40] Yashin, V. V., and Balazs, A. C., 2007, "Theoretical and Computational
- Modeling of Self-Oscillating Polymer Gels," J. Chem. Phys., 126(12), p. 124707.
- [41] Zhang, T., 2019, "Deriving a Lattice Model for Neo-Hookean Solids From Finite Element Methods," Extreme Mech. Lett., 26, pp. 40-45.
- [42] Ye, H., Li, Y., and Zhang, T., 2021, "Magttice: A Lattice Model for Hard-Magnetic Soft Materials," Soft Matter, 17(13), pp. 3560–3568.
- [43] Liu, D., Chen, C., and Zhang, T., 2021, "Image-Based Polygonal Lattices for Mechanical Modeling of Biological Materials: 2D Demonstrations," ACS Biomater. Sci. Eng.
- [44] Gao, H., and Yao, H., 2004, "Shape Insensitive Optimal Adhesion of Nanoscale Fibrillar Structures," Proc. Natl. Acad. Sci., 101(21), pp. 7851–7856.
- [45] Yao, H., Guduru, P., and Gao, H., 2008, "Maximum Strength for Intermolecular Adhesion of Nanospheres at an Optimal Size," J. R. Soc. Interface, 5(28), pp. 1363-1370.
- [46] Israelachvili, J. N., 2011, Intermolecular and Surface Forces, Academic Press, Burlington, MA.
- [47] Thompson, A. P., Aktulga, H. M., Berger, R., Bolintineanu, D. S., Brown, W. M., Crozier, P. S., in't Veld, P. J., et al., 2022, "LAMMPS—A Flexible Simulation Tool for Particle-Based Materials Modeling at the Atomic, Meso, and Continuum Scales," Comput. Phys. Commun., 271, pp. 108171.
- [48] Cao, Y., and Hutchinson, J. W., 2012, "Wrinkling Phenomena in Neo-Hookean Film/Substrate Bilayers," ASME J. Appl. Mech., 79(3), p. 031019.
- [49] Brau, F., Vandeparre, H., Sabbah, A., Poulard, C., Boudaoud, A., and Damman, P., 2011, "Multiple-Length-Scale Elastic Instability Mimics Parametric Resonance of Nonlinear Oscillators," Nat. Phys., 7(1), pp. 56–60.
 [50] Budday, S., Kuhl, E., and Hutchinson, J. W., 2015, "Period-Doubling and
- Period-Tripling in Growing Bilayered Systems," Philos. Mag., 95(28-30), pp. 3208-3224
- [51] Zhao, R., Zhang, T., Diab, M., Gao, H., and Kim, K.-S., 2015, "The Primary Bilayer Ruga-Phase Diagram I: Localizations in Ruga Evolution," Extreme Mech. Lett., 4, pp. 76–82.
- [52] Barquins, M., 1988, "Adherence and Rolling Kinetics of a Rigid Cylinder in Contact With a Natural Rubber Surface," J. Adhes., 26(1), pp. 1-12.

- [53] Chaudhury, M. K., Weaver, T., Hui, C., and Kramer, E., 1996, "Adhesive Contact of Cylindrical Lens and a Flat Sheet," J. Appl. Phys., 80(1), pp. 30-37.
- [54] Johnson, K. L., Kendall, K., and Roberts, A., 1971, "Surface Energy and the Contact of Elastic Solids," Proc. R. Soc. A: Math. Phys. Eng. Sci., 324(1558), pp. 301-313.
- [55] Zhou, M., 2003, "A New Look at the Atomic Level Virial Stress: on Continuum-Molecular System Equivalence," Proc. R. Soc. A, 459(2037), pp. 2347-2392.
- [56] Admal, N. C., and Tadmor, E. B., 2010, "A Unified Interpretation of Stress in Molecular Systems," J. Elast., 100(1-2), pp. 63-143.
- [57] Glassmaker, N. J., Jagota, A., Hui, C.-Y., Noderer, W. L., and Chaudhury, M. K., 2007, "Biologically Inspired Crack Trapping for Enhanced Adhesion," Proc. Natl. Acad. Sci., 104(26), pp. 10786-10791.
- [58] Lin, G., Chandrasekaran, P., Lv, C., Zhang, Q., Tang, Y., Han, L., and Yin, J., 2017, "Self-similar Hierarchical Wrinkles as a Potential Multifunctional Smart Window With Simultaneously Tunable Transparency, Structural Color, and Droplet Transport," ACS Appl. Mater. Interfaces, 9(31), pp. 26510–26517.
- [59] Chen, C., Airoldi, C. A., Lugo, C. A., Bay, R. K., Glover, B. J., and Crosby, A. J., 2021, "Flower Inspiration: Broad-Angle Structural Color Through Tunable Hierarchical Wrinkles in Thin Film Multilayers," Adv. Funct. Mater., 31(5), p. 2006256.
- [60] Nagashima, S., Suzuki, K., Matsubara, S., and Okumura, D., 2023, "Bio-Inspired Instability-Induced Hierarchical Patterns Having Tunable Anisotropic Wetting Properties," Adv. Mater. Interfaces, 10(14), p. 2300039.
- [61] Bowden, N., Brittain, S., Evans, A. G., Hutchinson, J. W., and Whitesides, G. M., 1998, "Spontaneous Formation of Ordered Structures in Thin Films of Metals Supported on an Elastomeric Polymer," Nature, 393(6681), pp. 146-149.
- [62] Genzer, J., and Groenewold, J., 2006, "Soft Matter With Hard Skin: From Skin Wrinkles to Templating and Material Characterization," Soft Matter, 2(4), pp. 310-323.
- [63] Cai, S., Breid, D., Crosby, A. J., Suo, Z., and Hutchinson, J. W., 2011, "Periodic Patterns and Energy States of Buckled Films on Compliant Substrates," J. Mech. Phys. Solids., 59(5), pp. 1094–1114.
- [64] Li, B., Cao, Y.-P., Feng, X.-Q., and Gao, H., 2012, "Mechanics of Morphological Instabilities and Surface Wrinkling in Soft Materials: A Review," Soft Matter, 8(21), pp. 5728-5745.
- [65] Yin, J., Yagüe, J. L., Eggenspieler, D., Gleason, K. K., and Boyce, M. C., 2012, Deterministic Order in Surface Micro-Topologies Through Sequential Wrinkling," Adv. Mater., 24(40), pp. 5441–5446. [66] Wang, Q., and Zhao, X., 2016, "Beyond Wrinkles: Multimodal Surface
- Instabilities for Multifunctional Patterning," MRS Bull., 41(02), pp. 115–122. [67] Yang, S., Khare, K., and Lin, P. C., 2010, "Harnessing Surface Wrinkle Patterns in Soft Matter," Adv. Funct. Mater., 20(16), pp. 2550-2564.
- [68] Ye, H., Shen, Z., Xian, W., Zhang, T., Tang, S., and Li, Y., 2020, "OpenFSI: A Highly Efficient and Portable Fluid-Structure Simulation Package Based on Immersed-Boundary Method," Comput. Phys. Commun., 256, p. 107463.
- [69] Diab, M., Zhang, T., Zhao, R., Gao, H., and Kim, K.-S., 2013, "Ruga Mechanics of Creasing: From Instantaneous to Setback Creases." Proc. R. Soc. A. 469. p. 20120753.
- [70] Zhao, R., Diab, M., and Kim, K.-S., 2016, "The Primary Bilayer Ruga-Phase Diagram ii: Irreversibility in Ruga Evolution," ASME J. Appl. Mech., 83(9),
- p. 091004. [71] Hohlfeld, E., and Mahadevan, L., 2011, "Unfolding the Sulcus," Phys. Rev. Lett.,
- 106(10), p. 105702. [72] Hong, W., Zhao, X., and Suo, Z., 2009, "Formation of Creases on the Surfaces of Elastomers and Gels," Appl. Phys. Lett., 95(11), p. 111901.
- [73] Gent, A., and Cho, I., 1999, "Surface Instabilities in Compressed or Bent Rubber Blocks," Rubber Chem. Technol., 72(2), pp. 253-262.
- [74] Sun, J.-Y., Xia, S., Moon, M.-W., Oh, K. H., and Kim, K.-S., 2012, "Folding Wrinkles of a Thin Stiff Layer on a Soft Substrate," Proc. R. Soc. A, 468, pp. 932-953.
- [75] Brau, F., Damman, P., Diamant, H., and Witten, T. A., 2013, "Wrinkle to Fold Transition: Influence of the Substrate Response," Soft Matter, 9(34), pp. 8177-
- [76] Zang, J., Zhao, X., Cao, Y., and Hutchinson, J. W., 2012, "Localized Ridge Wrinkling of Stiff Films on Compliant Substrates," J. Mech. Phys. Solids., 60(7), pp. 1265-1279.